MOMENTUM MANAGEMENT OF A SPACECRAFT EQUIPPED WITH A DUAL-GIMBALLED ELECTRIC THRUSTER

R. Calaon[*], L. Kiner[*], C. Allard[†]and H. Schaub[‡]

Spacecraft are often subject to unmodeled forces and torques which, even when small, can cause significant variations to the desired position and attitude in orbit. One of such effects is the solar radiation pressure, which manifests in the form of a nonzero net torque on the spacecraft. To maintain the desired attitude over time, such unmodeled torques must be compensated by the actuators, typically reaction wheels. Over long periods of time, the reaction wheel speeds grow significantly to compensate such torques, and the accumulated wheel momentum needs to be periodically dumped. This paper investigates the use of a Solar Electric Propulsion thruster, whose primary scope is to provide low thrust to follow a heliocentric trajectory. The thruster is mounted on a dual-gimballed platform attached to the spacecraft hub: the two degrees of freedom associated with the direction of the thruster are exploited to counteract the momentum build-up on the wheels, and reduce the necessity of performing momentum dumping.

INTRODUCTION

Modern spacecraft designs are often met with increasing power requirements to meet the needs of each subsystem. With the takeover of low-thrust electric propulsion to reduce fuel consumption and wet mass, the spacecraft needs to be able to produce enough power to sustain such electric thrusters. For spacecraft orbiting Earth, or orbiting the Sun within the inner part of the Solar System, this requirement ofter translates in the necessity of equipping the spacecraft with very large solar arrays to meet the power demand. This, on the other hand, makes the effects of the Solar Radiation Pressure (SRP) acting on the spacecraft system significantly stronger, as large solar arrays can act like solar sails that can cause the spacecraft to drift away from nominal attitude.[1] The attitude of the spacecraft is often designed to meet a series of pointing requirements, and therefore it must be maintained within a certain accuracy to allow for the mission to proceed nominally. For this reason, the torque resulting from SRP, as well as other unmodeled external torques, is typically absorbed by momentum exchange devices such as Reaction Wheels (RWs) or Control Moment Gyros (CMGs). These actuators can be spun up and down to exchange momentum with the spacecraft and perform attitude maneuvers or, conversely, they can hold the spacecraft attitude in place while absorbing external torques.[2] In the second case, because external torques are acting on the system, the angular momentum is accumulated on the actuators, rather than the spacecraft hub. This can be done up to a

certain point, because significant problems arise when RWs or CMGs are spun at very high angular rates. First of all, this causes mechanical stress on the bearings and significant power consumption. Second of all, a high accumulated momentum makes it increasingly harder to control the spacecraft, requiring a larger torque from the actuators, which might in return not be able to deliver it.

For the aforementioned reasons, momentum dumping is a necessary part of the mission design, when external torques are provided to the system such that the resulting variation of net momentum brings down the angular velocities of the wheels. In the most general case, this is done via a set of thrusters located on the main hub, typically in pairs to avoid producing net forces on the system that could cause trajectory deviations. This is obviously associated with additional propellant mass, and also with the problem of high-frequency oscillation resulting from the firing, which can excite the vibrational modes of long appendages such as the solar arrays[3] or require accurate positioning of the payload.[4] Another problem related to performing momentum dumping using thrusters is the fact that one or more of them might fail. For this reason, work exists in literature that addresses how to dump momentum using underactuated controls torques.[5] In this case, however, momentum dumping happens over multiple phases that require attitude reorientation, thus losing the reference attitude temporarily. Other existing work investigated how to perform momentum dumping continuously and exploiting environment features, such as the gravity gradient torque,[6] or Earth's magnetic field, by means of onboard magnetorquers.[7] Both these approaches, however, are only applicable for Earth-orbiting satellites, and not for deep-space missions.

This work considers a spacecraft on a heliocentric orbit, propelled by a Solar Electric Propulsion (SEP) thruster. The thruster is mounted on a platform that is connected to the spacecraft hub via a two-axes gimbal that allows it to perform tip-and-tilt type of rotations. Additionally, the spacecraft features two solar arrays attached to the hub via a one-degree-of-freedom hinges, which allow the arrays to rotate about the hinge axis to maximize the incidence of sunlight. The goal of this paper is to articulate the platform in order to align the thrust direction with the center of mass, when the desire is to not produce a net torque on the system. As a direct consequence, this paper looks into designing a control algorithm that can align the thruster at an offset with respect to the system's center of mass, in order to have the nonzero torque counteract the momentum building up on the wheels due to SRP. A similar concept has been proposed for the Psyche mission, involving two such thrusters mounted each onto a gimbl.[8] Simulating such a complex collection of spacecraft-related phenomena is not trivial. To fulfil this purpose, this work relies on the University of Colorado's Basilisk Astrodynamics Simulation Framework[*]. This software allows to combine multiple segments of code, each of which executes an individual element of the simulation, whether that is flight software or simulated spacecraft hardware. The full simulation, comprising all the building blocks, considers all the couplings between the different components, and guarantees high-fidelity standards.

This paper is structured as follows: first, an overview of Basilisk is provided, where the main building blocks of the simulation, or modules, are presented, highlighting the interconnected nature of the problem. Secondly, the mass and inertia properties of the spacecraft hub and rotating appendages are presented, together with the specifications about the SEP thruster. A brief section explains how the SRP torque is modeled. The main section of the paper describes the motion of the platform and its constraints, and derives an algorithm to align the platform with a desired point on the hub, as well as a control scheme to use the torque produced by the thruster to continuously dump the momentum on the wheels. The second-to-last section of the paper shows some numerical

---

[*] http://hanspeterschaub.info/basilisk

2
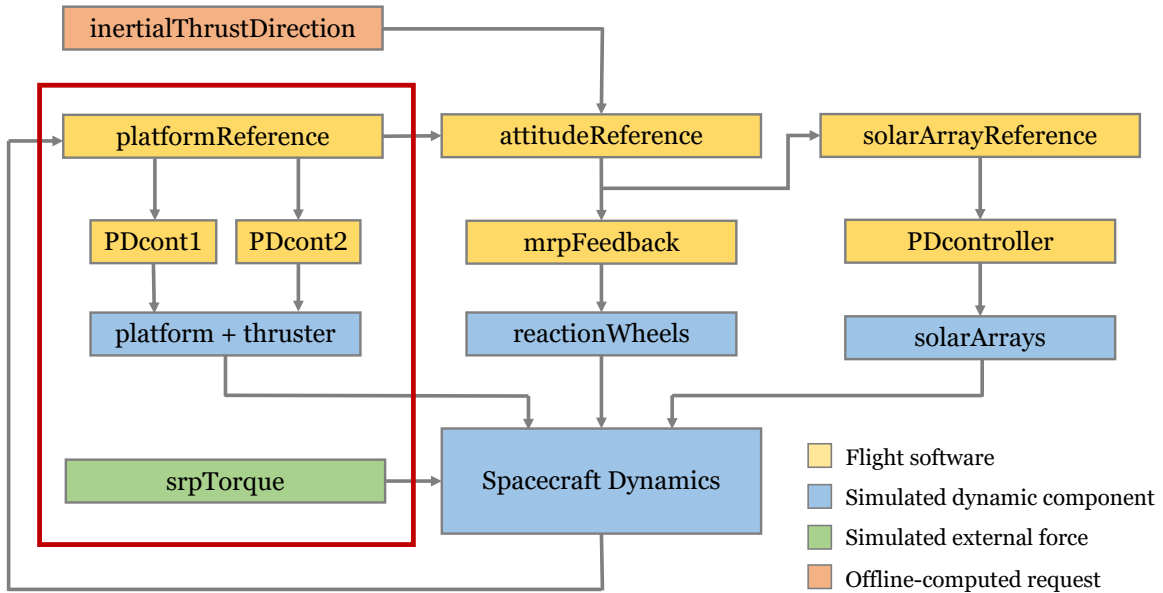
Figure 1: Simulation block diagram

results for different case scenarios. Ultimately, conclusions are drawn.

SIMULATION FRAMEWORK

Basilisk is an open-source software framework that can simulate complex spacecraft systems and behaviors. Its strength relies in its dual nature, consisting in a Python-scripted interface and a C/C++ core. The Python surface layer enables the user to easily connect different segments of code, which can be added as the building blocks of an increasingly complex simulation. The underlying C/C++ core, on the other hand, ensures execution speed. The second key feature of Basilisk's design is its modular structure, which allows for such building blocks, named modules, to exist as standalone segments of code, with minimal interconnections. This modular structure is enabled by the messaging system, thanks to which each module receives input messages from other modules and writes output messages to other modules, limiting the flow of information to what is strictly essential[9, 10]

Figure 1 illustrates the most relevant modules that are used in the simulations carried out in this paper. Flight software modules contain code that would be run by an onboard computer, to calculate the required controls that are to be given to the actuators, based on the information on the spacecraft state provided by sensors. In blue are modules that simulate dynamical components of the spacecraft, such as reaction wheels, solar arrays, and the spacecraft itself. In a real scenario, these modules are replace by hardware components. In green is a module that simulates the Solar Radiation Pressure (SRP) torque acting on the spacecraft. Lastly, in orange, is a module that outputs the requested inertial direction for the thrust vector, required in order to track the precomputed thrust interplanetary trajectory. The gray arrows describe the flow of information between modules, as well as how each component of the simulation affects the others.

This paper primarily focuses on the control and actuation of the platform and thruster assembly, and the effect that these have on the whole system: these building blocks described in the future sections are those contained in the red box in Figure 1. Despite this, looking at Figure 1 in its entirety is important in order to understand the problem as a whole, and the deep network of interconnections by which it is characterized. The `platformReference` module outputs reference angles for the platform motion. Such angles are computed based on the location of the center of mass of the system, which comes from the spacecraft dynamical model. In this work, the position of the center of mass of the system is assumed to be known exactly. In reality this is not the case, and the coordinates of the center of mass would have to be estimated. As Reference 8 points out, this is a problem when the desire is to have the thruster aligned with the center of mass; when, however, continuous momentum dumping is performed, the offset with respect to the center of mass makes uncertainties on its position less relevant. The platform reference is computed based the position of the center of mass; the reference angles are tracked by some PD controllers, which output the torques that control the platform and thruster assembly. As a consequence, the motion of the thruster with respect to the hub produces a torque on the system that affects the spacecraft dynamics. Moreover, the `platformReference` outputs a reference direction for the thrust vector with respect to the spacecraft hub. This information is used by the `attitudeReference` module to align such direction with the requested `inertialThrustDirection`. Based on the error between current attitude and reference attitude, a torque request is computed and fed to the `reactionWheels`, which actuate the spacecraft. Additionally, the `solarArrayReference` module computes a reference for the rotating solar arrays in order to ensure best lighting condition. The motion of the solar arrays also affects the spacecraft hub. Lastly, the `srpTorque` acts directly on the spacecraft as a whole, in the form of an external torque that can cause it to drift away from the required attitude.

The diagram in Figure 1 summarized the main blocks involved in the simulation. For a more detailed analysis of the reference-tracking routines and the interconnections between effectors and spacecraft hub, the reader is redirected to.[9, 11]

SPACECRAFT MODELING

The spacecraft analyzed in this paper is modeled as the assembly of multiple rigid bodies connected to one-another. The spacecraft hub is modeled as a cube with a 1.5 m side, a mass $m = 750$ kg and the following inertia tensor, expressed with respect to a principal frame $\mathcal{B}$:

$$
{}^{\mathcal{B}}[\boldsymbol{I}_{sc}] = \begin{bmatrix} 900 & 0 & 0 \\ 0 & 800 & 0 \\ 0 & 0 & 600 \end{bmatrix} \text{ kg m}^2. \tag{1}
$$

The spacecraft is actuated by means of four reaction wheels in a pyramid configuration as shown in Figure 2, with the spin axes $\hat{\boldsymbol{u}}_j$ having one component along each of the four axes $\pm{}^{\mathcal{B}}\hat{\boldsymbol{b}}_x = (\pm 1, 0, 0)^T$ and $\pm{}^{\mathcal{B}}\hat{\boldsymbol{b}}_y = (0, \pm 1, 0)^T$, and tilted upwards 40 deg to provide control about the ${}^{\mathcal{B}}\hat{\boldsymbol{b}}_z = (0, 0, 1)^T$ axis. The wheels have a mass of 12 kg and a moment of inertia $I_\omega = 0.08$ kg m^2, and each and can provide torques up to 0.2 Nm and have a maximum wheel speed of 6000 rpm.

The two solar arrays are connected through a one-degree-of-freedom hinge, attached to the upper surface of the hub and along the principal axis ${}^{\mathcal{B}}\hat{\boldsymbol{b}}_x = (1, 0, 0)^T$, in both directions. The degree of freedom of the hinges allows the arrays to rotate about these axes to maximize sun incidence on the power-generating surface. The arrays are modeled as thin discs with a diameter of 7 m, whose center of mass is located at 3.75 m from the hinges. The mass of the solar arrays is $m_{sa} = 5$ kg and
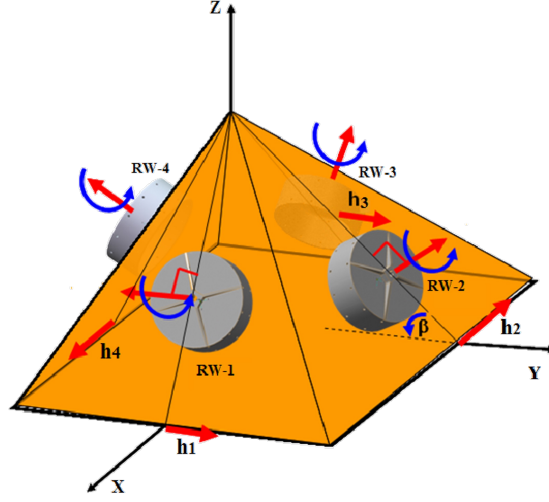
Figure 2: Four reaction wheels in pyramid configuration

the inertia tensor is:

$$
{}^{\mathcal{S}}[\boldsymbol{I}_{sa}] = \begin{bmatrix} 17.5 & 0 & 0 \\ 0 & 35 & 0 \\ 0 & 0 & 17.5 \end{bmatrix} \text{ kg m}^2 \tag{2}
$$

with respect to a principal frame $\mathcal{S}$.

The platform and thruster assembly is treated as a rigid body with negligible mass, attached to the lower surface of the spacecraft. A two axis gimbal connects the platform to the main hub, allowing it to perform tip and tilt rotations with respect to the hub. A more detailed description of the platform gimbal and its constrained motion is provided in the following sections. The thruster is assumed to fire continuously, with a specific impulse $I_{sp} = 1600$ s and a thrust output of $t = 0.1$ N.

SOLAR RADIATION PRESSURE MODELING

For the purpose of SRP modeling, the spacecraft is represented as a collection of 10 facets with negligible thickness. Six square facets and four circular facets are used to model the rigid hub and solar arrays, respectively. The platform and thruster assembly are not considered for the SRP evaluation due to their relatively small size compared to the spacecraft hub and solar arrays.

Each facet is characterized by an area A, a vector normal to its surface $\hat{\boldsymbol{n}}$, a position vector from the spacecraft center of mass to the facet center of pressure, $\boldsymbol{r}_{F/c}$, and three optical coefficients representing the interaction of impinging photons with the facet surface. The fraction of specularly reflected, diffusely scattered, and absorbed photons are represented using the coefficients δ, ρ, and α, respectively.

A faceted force model is used to estimate the SRP force acting on the spacecraft:[12]

$$
\boldsymbol{F}_{SRP} = \sum_{i=1}^{10} \boldsymbol{F}_{SRP_i} = -P(|\boldsymbol{r}_{sc/\odot}|) \sum_{i=1}^{10} A_i \cos(\theta_i) \left[(1 - \delta_i)\hat{\boldsymbol{s}} + 2 \left(\frac{\rho_i}{3} + \delta_i \cos(\theta_i) \right) \hat{\boldsymbol{n}}_i \right] \tag{3}
$$

5

where $\hat{s}$ is the unit direction vector pointing radially towards the Sun from the spacecraft body-frame origin, θ is defined as the incidence angle between each facet normal vector and the Sun-direction vector, and $P(|\boldsymbol{r}_{sc/\odot}|)$ is the pressure acting on the spacecraft scaled by the spacecraft heliocentric distance. The vector quantities in Equation (3) are expressed in spacecraft principal body-frame components. The total torque acting on the spacecraft center of mass due to SRP is calculated by summing the torque contributions over all 10 facets:

$$\boldsymbol{L}_{SRP,c} = \sum_{i=1}^{10} \boldsymbol{L}_{SRP,c_i} = \sum_{i=1}^{10} \boldsymbol{r}_{F_i/c} \times \boldsymbol{F}_{SRP_i}. \tag{4}$$

PLATFORM REFERENCE GENERATION

The platform is modeled as a rigid body attached to the main spacecraft hub. To describe the relative motion between the two, two frames are defined: frame $\mathcal{M} = \{\hat{\boldsymbol{m}}_1, \hat{\boldsymbol{m}}_2, \hat{\boldsymbol{m}}_3\}$ is a hub-fixed frame, whose origin M coincides with the joint through which the platform and hub are connected and exchange forces. Frame $\mathcal{F} = \{\hat{\boldsymbol{f}}_1, \hat{\boldsymbol{f}}_2, \hat{\boldsymbol{f}}_3\}$, with origin F, is a platform-fixed frame. The relative motion between the platform and the hub consists of 2 degrees of freedom tip-and-tild rotations. Such rotation angles ν_1 and ν_2 are defined about the $\hat{\boldsymbol{m}}_1$ axis and the intermediate $\hat{\boldsymbol{f}}_2$ axis, respectively, via two consecutive rotations. The direction cosine matrix that defines the mapping from $\mathcal{M}$ to $\mathcal{F}$ is therefore:

$$[\mathcal{FM}] = \begin{bmatrix} \cos\nu_2 & \sin\nu_1\sin\nu_2 & -\cos\nu_1\sin\nu_2 \\ 0 & \cos\nu_1 & \sin\nu_1 \\ \sin\nu_2 & -\sin\nu_1\cos\nu_2 & \cos\nu_1\cos\nu_2 \end{bmatrix} \tag{5}$$
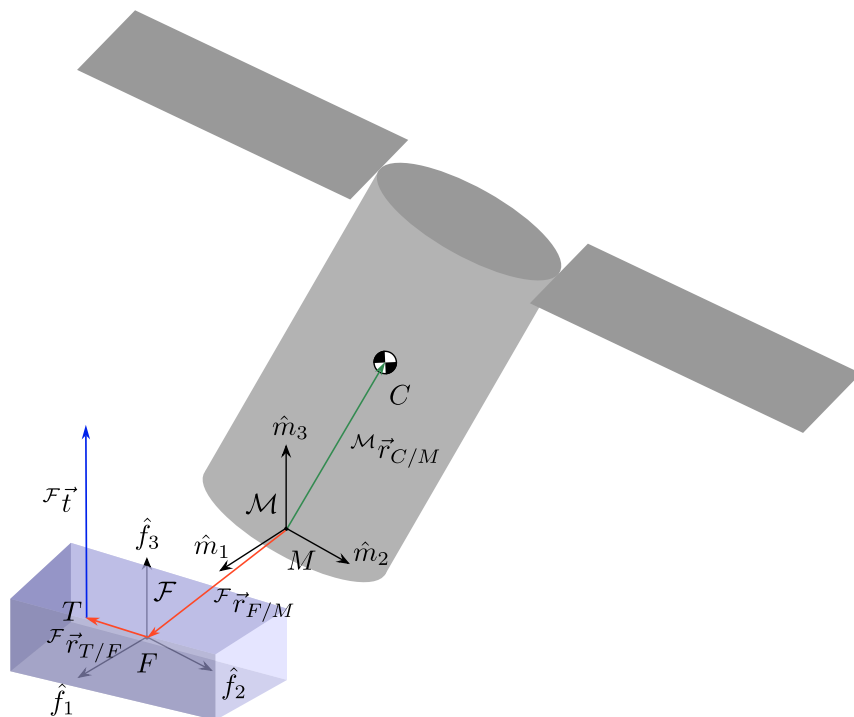
Figure 3: Hub and platform, with relative frames $\mathcal{M}$ and $\mathcal{F}$ and offsets

6

where emphasis is put on the fact that the element $(2, 1)$ of the $[\mathcal{FM}]$ direction cosine matrix must be zero. This ensures that the rotation is, in fact, a tip-and-tilt type of rotation that is compliant with the constrained motion of the platform. Moreover, it can be observed that when $\nu_1 = \nu_2 = 0$ the two frames align and the mapping becomes an identity. Figure 3 shows a sketch of the spacecraft hub and the platform, and the relative frames.

The complexity of the problem involving the articulation of the platform lies in the fact that the thrust vector is expressed in $\mathcal{F}$ frame coordinates and applied through point T, which may not coincide with the origin F of the frame. Additionally, the origins of the two frames, M and F, do not, in general, coincide either. This section describes how to compute the rotation angles ν_1 and ν_2 that allow to put the thrust direction vector $^{\mathcal{F}}\boldsymbol{t}$, expressed in $\mathcal{F}$-frame coordinates, through a specific point C in the hub. This point C can coincide with the system's center of mass, if the desire is to have the thrust not produce a torque on the system. Vice versa, it is possible to intentionally thrust at an offset distance from the center of mass to exploit such torque to perform momentum dumping. To solve the problem in its most general form, the following offset vectors are defined:

- $^{\mathcal{M}}\boldsymbol{r}_{C/M}$: position of C with respect to M, expressed in $\mathcal{M}$-frame coordinates;

- $^{\mathcal{F}}\boldsymbol{r}_{F/M}$: position of F with respect to M, expressed in $\mathcal{F}$-frame coordinates;

- $^{\mathcal{F}}\boldsymbol{r}_{T/F}$: position of T with respect to F, expressed in $\mathcal{F}$-frame coordinates.

The final direction cosine matrix that aligns the thrust with the desired point C is obtained via a series of three consecutive rigid body rotations that take advantage of intermediate frames. For ease of notation, the following vector are defined and used in the following subsections:

$$\boldsymbol{a} = \boldsymbol{r}_{F/M} + \boldsymbol{r}_{T/F} \qquad\qquad \boldsymbol{b} = \boldsymbol{r}_{C/M}. \qquad (6)$$

First rotation

The first rotation is defined starting from the hub-fixed frame $\mathcal{M}$, and it maps to an intermediate frame $\mathcal{D}_1$ such that, when $\mathcal{F} \equiv \mathcal{D}_1$, the thrust vector $\boldsymbol{t}$ is parallel to $\boldsymbol{b}$. The DCM $[\mathcal{D}_1\mathcal{M}]$ is defined by means of principal rotation angle and principal rotation vector $(\phi, \hat{\boldsymbol{e}}_\phi)$. These quantities are computed as follows:

$$\phi = \arccos\left(\frac{^{\mathcal{F}}\boldsymbol{t} \cdot {}^{\mathcal{M}}\boldsymbol{b}}{\|\boldsymbol{t}\| \cdot \|\boldsymbol{b}\|}\right) \qquad\qquad \hat{\boldsymbol{e}}_\phi = \frac{^{\mathcal{F}}\boldsymbol{t} \times {}^{\mathcal{M}}\boldsymbol{b}}{\|^{\mathcal{F}}\boldsymbol{t} \times {}^{\mathcal{M}}\boldsymbol{b}\|}. \qquad (7)$$
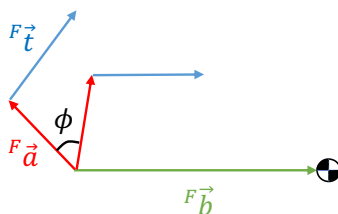
Figure 4: First rotation visualized

Defining $\Sigma = 1 - \cos\phi$ and $\hat{\boldsymbol{e}}_\phi = (e_1, e_2, e_3)^T$, the first rotation DCM is obtained as:

$$[\mathcal{D}_1\mathcal{M}] = \begin{bmatrix} e_1^2\Sigma + \cos\phi & e_1e_2\Sigma + e_3\sin\phi & e_1e_3\Sigma - e_2\sin\phi \\ e_1e_2\Sigma - e_3\sin\phi & e_2^2\Sigma + \cos\phi & e_2e_3\Sigma + e_1\sin\phi \\ e_1e_3\Sigma + e_2\sin\phi & e_2e_3\Sigma - e_1\sin\phi & e_3^2\Sigma + \cos\phi \end{bmatrix}. \tag{8}$$

Figure 4 visually shows the rotation of vectors performed by the first DCM. It should be noted that the matrix computed in Equation (8) is, in general, not constraint compliant, i.e., it does not describe a tip-and-tild rotation like the DCM outlined in Equation (5).

Second rotation

The second rotation puts the thrust direction vector through point C. The principal rotation vector in this case is again $\hat{\boldsymbol{e}}_\psi = \hat{\boldsymbol{e}}_\phi$, so the rotation is a direct continuation of the previous one. The derivation of the second principal rotation angle ψ, however, is significantly less intuitive. It should be pointed out that, when the thrust application point T coincides with the origin of the hub-fixed frame M, therefore $\|\boldsymbol{a}\| = 0$, it is also $\psi = 0$, and the first rotation alone is sufficient to put the thrust through point C. When this is not the case, the nonzero value of ψ must be computed.
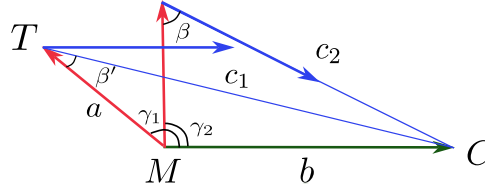
Figure 5: First rotation visualized

Figure 5 shows the second rotation that aligns the thrust vector, in blue and initially parallel to $\boldsymbol{b}$, to point C. The principal rotation angle ψ is obtained as $\psi = \gamma_1 - \gamma_2$. The angles β, β' and γ_1 are known from the geometry and the relative position of the vectors at the beginning of the second rotation. The segments c_1 and c_2, respectively the distance between the thrust application point T and point C before and after the rotation, are computed as follows:

$$c_1 = \sqrt{a^2 + b^2 - 2ab\cos\gamma_1} \qquad c_2 = a\cos\beta \pm \sqrt{b^2 - a^2\sin^2\beta}. \tag{9}$$

It is possible to observe that c_2 only exists when the relation $b \geq a|\sin\beta|$ is satisfied. This means that it might not always possible to align the thrust vector with point C for any choices of vectors $\boldsymbol{a}$ and $\boldsymbol{b}$. Taking the product of the two solutions for c_2 given in Equation (9) gives:

$$c_{2,1} \cdot c_{2,2} = a^2\cos^2\beta - b^2 + a^2\sin^2\beta = a^2 - b^2 \tag{10}$$

which is negative when $a < b$. This is considered a valid assumption for the following reasons: vector $\boldsymbol{b}$ indicates the position of point C, which in general coincides with the center of mass of the system, with respect to point M. For a massive spacecraft, the center of mass of the system is located close to the geometric center of the system, thus away from the point M, which is at the lower end of the hub where the platform is attached. Vector $\boldsymbol{a}$, instead, is the offset between the

thrust application point T and point M. Assuming that the platform is relatively small compared to the spacecraft hub, it makes sense to assume that $a < b$ is respected. With these considerations, the choice for c_2 is:

$$c_2 = a\cos\beta + \sqrt{b^2 - a^2\sin^2\beta} \tag{11}$$

to ensure positivity. At this point, the rotation angle γ can be derived from trigonometric relations:

$$\begin{aligned}
\sin\psi = \sin(\gamma_1 - \gamma_2) &= \cos\gamma_2\sin\gamma_1 - \cos\gamma_1\sin\gamma_2 \\
&= \frac{1}{b}(c_1\cos\gamma_2\sin\beta' - c_2\cos\gamma_1\sin\beta)
\end{aligned} \tag{12}$$

with:

$$\cos\gamma_i = \frac{a^2 + b^2 - c_i^2}{2ab} \qquad \text{for} \qquad i = 1, 2. \tag{13}$$

Ultimately, the second DCM $[\mathcal{D}_2\mathcal{D}_1]$ is obtained applying Equation (8) with the principal rotation angle and vector $(\psi, \hat{e}_\psi)$. Multiplying the first and second rotation matrices gives the matrix:

$$[\mathcal{D}_2\mathcal{M}] = [\mathcal{D}_2\mathcal{D}_1][\mathcal{D}_1\mathcal{M}] \tag{14}$$

where it should be noted that again, in general, $[\mathcal{D}_2\mathcal{M}]$ does not describe a rotation that is compliant with the constraints expressed by Equation (5).

Third Rotation

The first two rotations show that it is possible, under reasonable assumptions, to rotate the thrust vector in order to align it with point C in the hub. However, it is not yet possible to do so through a rotation that is also compliant with the platform's constraints, which only allow it to perform tip-and-tilt kind of rotations. This subsection computes a third rotation DCM that maintains the alignment condition achieved by the first two rotations, and simultaneously enforces the constraint compliance on the final solution.
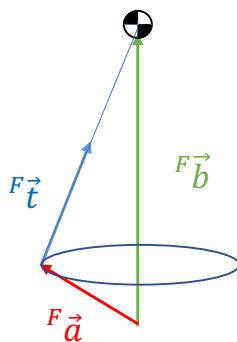
Figure 6: Third rotation visualized

Equation (14) provides a rotation matrix that puts the thrust vector through point C, but this rotation is not unique. In fact, there exists a family of infinite DCMs that do the same. Of all such DCMs, the purpose of this section is to find the one that is also constraint-compliant. Let's define such DCM $[\mathcal{D}_3\mathcal{M}]$. Figure 6 shows that rotations about the $\boldsymbol{b}$ vector do not break the desired alignment of the thrust vector. For this reason, the principal rotation vector of the third rotation, $\hat{\boldsymbol{e}}_\theta$, is defined as:

$$\hat{\boldsymbol{e}}_\theta = \frac{\boldsymbol{b}}{\|\boldsymbol{b}\|}. \tag{15}$$

The unknown variable in this problem is the principal rotation angle θ. Let's define the Gibb's vector, or Classic Rodrigues Parameter (CRP) vector:

$$\boldsymbol{q} = \hat{\boldsymbol{e}}_\theta \tan\left(\frac{\theta}{2}\right) \tag{16}$$

from which the third DCM is expressed as:

$$[\mathcal{D}_3\mathcal{D}_2] = \frac{1}{1 + \boldsymbol{q}^T \boldsymbol{q}} \begin{bmatrix} 1 + q_1^2 - q_2^2 - q3^2 & 2(q_1 q_2 + q_3) & 2(q_1 q_3 - q_2) \\ 2(q_1 q_2 + q_3) & 1 - q_1^2 + q_2^2 - q3^2 & 2(q_2 q_3 + q_1) \\ 2(q_1 q_3 + q_2) & 2(q_2 q_3 - q_1) & 1 - q_1^2 - q_2^2 + q3^2 \end{bmatrix}. \tag{17}$$

The goal is to obtain a final DCM $[\mathcal{F}\mathcal{M}]$ such that:

$$[\mathcal{F}\mathcal{M}] = [\mathcal{D}_3\mathcal{M}] = [\mathcal{D}_3\mathcal{D}_2][\mathcal{D}_2\mathcal{D}_1][\mathcal{D}_1\mathcal{M}] \tag{18}$$

is of the same form as Equation (5). Defining the following quantities component-wise:

$$\hat{\boldsymbol{e}}_\theta = (e_1, e_2, e_3)^T \qquad\qquad [\mathcal{D}_2\mathcal{M}] = \begin{bmatrix} d_{11} & d_{12} & d_{13} \\ d_{21} & d_{22} & d_{23} \\ d_{31} & d_{32} & d_{33} \end{bmatrix}, \tag{19}$$

carrying out the product $[\mathcal{D}_3\mathcal{M}] = [\mathcal{D}_3\mathcal{D}_2][\mathcal{D}_2\mathcal{M}]$ and equating the element $(2, 1)$ of $[\mathcal{D}_3\mathcal{M}]$ to zero to meet the rotational constraint, gives the following equation:

$$\frac{At^2 + Bt + C}{1 + t^2} = 0 \qquad\qquad \text{with} \qquad\qquad t = \tan\left(\frac{\theta}{2}\right) \tag{20}$$

where:

$$\begin{aligned} A &= 2(d_{21} e_2^2 + d_{11} e_1 e_2 + d_{31} e_2 e_3) - d_{21} \\ B &= 2(d_{31} e_1 - d_{11} e_3) \\ C &= d_{21}. \end{aligned} \tag{21}$$

Equation (20) has solutions when $\Delta = B^2 - 4AC \geq 0$. In such case, it is obviously:

$$t = \frac{-B \pm \sqrt{\Delta}}{2A} \tag{22}$$

which can be plugged back into Equation (16) and subsequently into Equation (17) to obtain $[\mathcal{D}_3\mathcal{D}_2]$. Finally, Equation (18) yields the rotation $[\mathcal{F}\mathcal{M}]$ that complies with all the requirements. Defining f_{ij} for $i, j = 1, 2, 3$ the elements of the $[\mathcal{F}\mathcal{M}]$ matrix, the tip and tilt angles ν_1 and ν_2 in Equation (5) are obtained as:

$$\nu_1 = \arctan\left(\frac{f_{23}}{f_{22}}\right) \qquad\qquad \nu_2 = \arctan\left(\frac{f_{31}}{f_{11}}\right). \tag{23}$$

10

Momentum dumping offset

The previous subsections showed how, by means of three consecutive rigid body rotations, it is possible to align the thrust vector with a point C on the hub. This point C can coincide with the center of mass of the whole system: in such case, the thrust does not produce any torque on the system. On the contrary, it is possible to intentionally offset the thrust vector from the center of mass to use the resulting torque to perform momentum dumping.

Let's define as $\Delta \boldsymbol{H}$ the amount of momentum that needs to be dumped. This can be a fraction of the momentum on the wheels that exceeds a certain threshold, or it can coincide with the total momentum on the wheels. In this application $\Delta \boldsymbol{H} = -\boldsymbol{H}$, i.e. the goal is to dump the entire net momentum on the wheels until their speeds are, ideally, brought to zero. The total net wheel momentum is computed as:

$$\boldsymbol{H} = \sum_{j=1}^{4} I_{\omega_j} \Omega_j \hat{\boldsymbol{u}}_j. \tag{24}$$

where I_{ω_j} is the inertia tensor of each wheel about the spin axis, Ω_j is the wheel speed and $\hat{\boldsymbol{u}}_j$ the spin axis. Let's define $\boldsymbol{d}$ as the offset vector from the center of mass, required to produce a torque $\boldsymbol{T}$ on the system. Over an infinitesimal time interval $\Delta\tau$ it is:

$$\Delta\boldsymbol{H} = \boldsymbol{T}\Delta\tau = \boldsymbol{d} \times \boldsymbol{t}\Delta\tau. \tag{25}$$

To obtain $\boldsymbol{d}$, both sides of the previous equation are cross-multiplied by $\boldsymbol{t}$. With the assumption that $\boldsymbol{d} \perp \boldsymbol{t}$, this gives:

$$\boldsymbol{t} \times \Delta\boldsymbol{H} = \boldsymbol{t} \times (\boldsymbol{d} \times \boldsymbol{t})\Delta\tau = [t^2\boldsymbol{d} - (\boldsymbol{t} \cdot \boldsymbol{d})\boldsymbol{t}]\Delta\tau = t^2\boldsymbol{d}\Delta\tau \tag{26}$$

which ultimately yields the control law:

$$\boldsymbol{d} = \frac{\kappa}{t^2}(\boldsymbol{t} \times \Delta\boldsymbol{H}) \tag{27}$$

where $\kappa = 1/\Delta\tau$ is a proportional control gain. A few assumptions have been made in this derivation. The coordinates of $\boldsymbol{t}$ are only known in the $\mathcal{F}$ frame, and in the $\mathcal{M}$ frame when the tip-and-tilt angles ν_1 and ν_2 are known. That is to say that the $\boldsymbol{t}$ vector that appears in Equation (27) is aligned with the system's center of mass, and the $\boldsymbol{d}$ vector computed accordingly is perpendicular to such direction, as shown in Figure 7. Offsetting the center of mass C by $\boldsymbol{d}$ gives point D, which is the point through which the thrust vector must fire in order to produce a torque that dumps the desired amount of momentum. Doing so requires reorienting the platform, thus changing the direction of $\boldsymbol{t}$. It can however be noted that this kind of continuous momentum dumping operates over large time scales, because it is over such long time scales that the effects of SRP become noticeable. For this reason is it safe to assume that the desired offset $\boldsymbol{d}$ is small, and consequently close to perpendicular to the thrust vector $\boldsymbol{t}$ resulting from the realignment of the platform through point D.

Another noteworthy aspect of Equation (27) consists in the fact that the resulting torque is always perpendicular to the line that connects points T and C. This means that if the momentum to be dumped $\Delta\boldsymbol{H}$ has a component along such direction, that component cannot be dumped. For this reason, this control law is not guaranteed to be always able to dump the required amount of momentum.
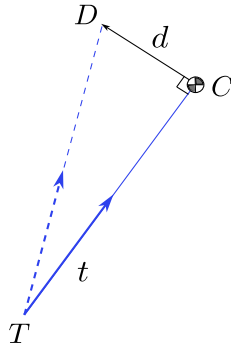
Figure 7: Center of mass offset

NUMERICAL RESULTS

This section shows the implementation of the platform reference generation algorithm into simulation. Because SRP forces and torques acting on the spacecraft are very small, it is necessary to run the simulation for several days to appreciate certain effects.

In these examples the spacecraft is in a heliocentric orbit, and it is initially performing a reorientation maneuver to acquire the desired attitude that can align the solar array normal with the Sun direction. Simultaneously, the reference is computed in order to make the thrust direction t aligned with an inertial direction that must be targeted to remain on the desired interplanetary trajectory. This has an important impact on the system as a whole, because as a results, the attitude reference and the platform reference are coupled, and therefore rapid changes in the platform angle references cause rapid changes in the attitude that is being targeted.

Attitude is controlled via a PID-like control law that zeroes the attitude error between the current body frame $\mathcal{B}$ and the reference frame $\mathcal{R}$, as well as the relative angular velocity $\boldsymbol{\omega}_{\mathcal{B}/\mathcal{R}}$. The reference angles for the platform are generated using the algorithm outlined in the previous section, while the platform is initially at a zero configuration with the $\mathcal{F}$ frame aligned with the $\mathcal{M}$ frame. The platform angles are also controlled via a PD controller that zeroes the error with the generated references. At the initial time, all wheel speeds are zero. All the control loops, as well as the attitude reference generation algorithm and the platform reference generation algorithm, are run at the same frequency of 1 Hz.

Short-term effects

This first scenario is run for one hour and it is meant to show the behavior of the spacecraft, the actuators, and the platform, in the short term, when the initial reorientation maneuver is performed. SRP is not applied in this scenario, and the gain κ of the momentum dumping control loop is set to zero. Figure 8 summarizes the most relevant features of this case. Subfigure (a) shows that the reference attitude, expressed in MRPs, is achieved in about 10 minutes, where dashed lines indicate reference coordinates. Subfigure (b) shows the platform angles tracking the reference angles, where dashed lines also represent reference quantities. Subfigure (c) shows that the wheels are actuated during the reorientation maneuver, and after that, the wheel speeds return to a near-zero value. Emphasis is given to the fact that, after the maneuver, the wheel speeds remain constant: because SRP is not acting on the system, there is no further need to actuate the spacecraft. Lastly, subfigure

(d) shows the angular offset between the system's center of mass and the thrust vector: it can be observed that, as the platform tracks the reference angles, such offset goes to zero, as no momentum management is performed in this scenario.

(a) Attitude and attitude reference vs time

(b) Platform angles and reference vs time

(c) Wheels speeds vs time

(d) Angular thruster - CM offset vs time
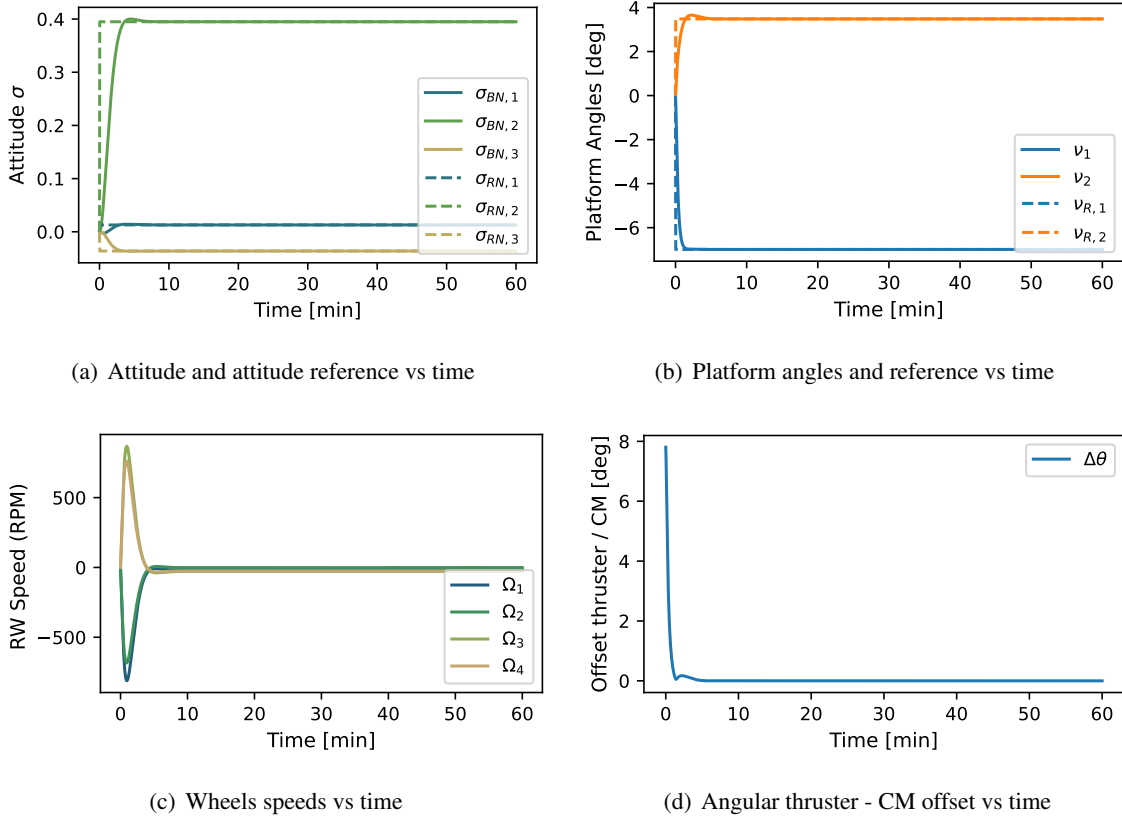
Figure 8: Short-term effects

Long-term SRP effect without momentum management

This second scenario adds the SRP modelling to the simulation, which is run for a week. No momentum management is performed, as the purpose of this scenario is to illustrate the effect of SRP on the spacecraft. The resulting plots are shown in Figure 9. Regarding subfigures (a), (b), and (d), the same behavior can be observed as in Figure 8, where reference attitude an platform angles are tracked and the center of mass offset is zeroed in the first few minutes of the simulation. Significantly different is subfigure (c), which shows the impact that SRP has on the reaction wheels over long periods of time. The SRP torque acting on the spacecraft is counteracted by the reaction wheels, which manage to hold the attitude in place. In return, to absorb such SRP torque, the wheels spin up. In a week's time, the wheels reach speeds above 2000 rpm each, which can cause significant mechanical stress on the bearings, excessive power consumption, and difficulty in using the wheels to effectively provide control torques. Subfigure (c) shows that the angle between the thrust vector and the net momentum H on the wheels, which over time settles around 90 deg.
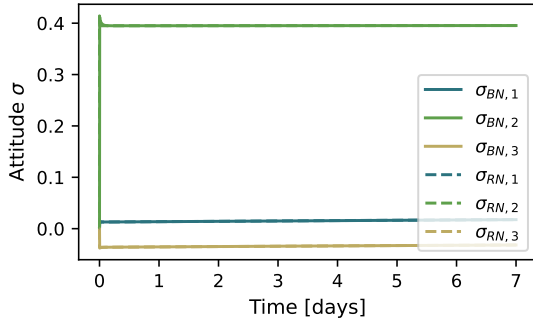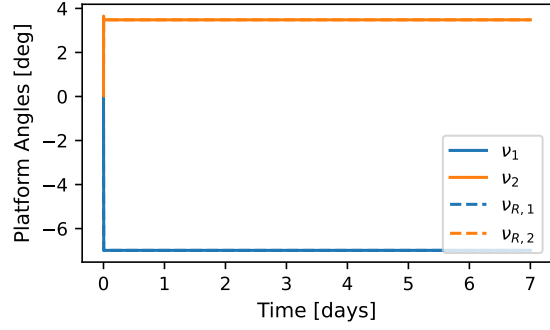
13

(a) Attitude and attitude reference vs time

(b) Platform angles and reference vs time
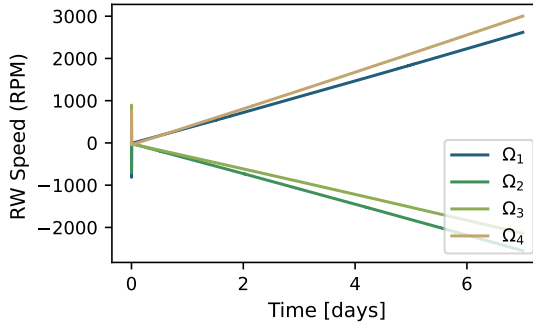
(c) Wheels speeds vs time
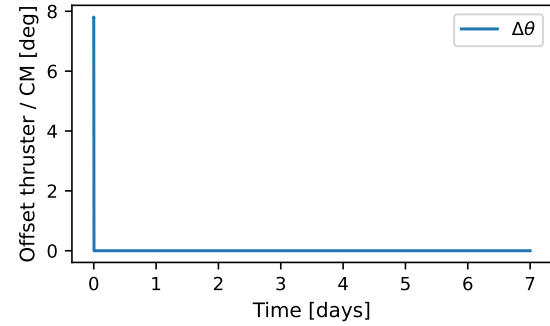
(d) Angular thruster - CM offset vs time
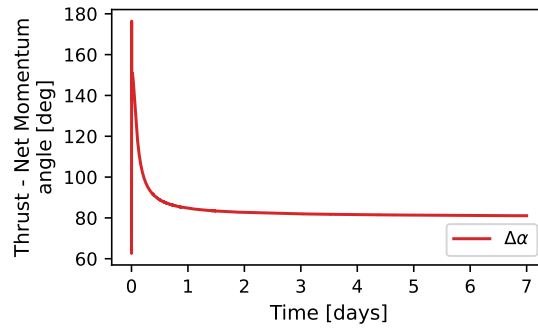
(e) Angular thruster - net momentum offset vs time

Figure 9: Long-term SRP effect, $\kappa = 0$

Long-term SRP effect with momentum management

The third scenario shows the effect of the momentum management algorithm outlined in the previous section when the system is subject to SRP torque. The gain used is $\kappa = 10^{-4}$ Hz. The results are reported in Figure 10. Subfigures (a) and (b) do not show significant differences. On the contrary, the most interesting result is displayed by subfigure (c): when the momentum management control loop is applied over the same time interval of a full week, the wheel speeds grow significantly less than they do in Figure 9. Where in the case without momentum management wheel

14

speeds reach above 2000 rpm, in this case all the wheels remain below 500 rpm. Another element of difference is that, in the previous case, wheels 2 and 3 had negative angular velocities. In the current scenario, however, all wheels have positive angular velocities. Subfigure (e) also shows an interesting, expected result: when the momentum management control loop is applied, the angle between thrust vector an net momentum H progressively decreases, down to approximately 6 deg after 7 days. This means that subfigure (c) is indeed showing the residual velocities that constitute the component of H that is along the direction that cannot be controlled by the momentum man-
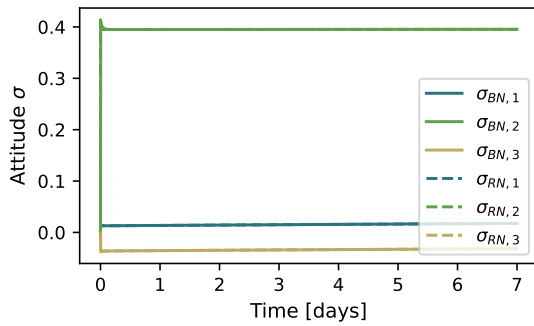
(a) Attitude and attitude reference vs time
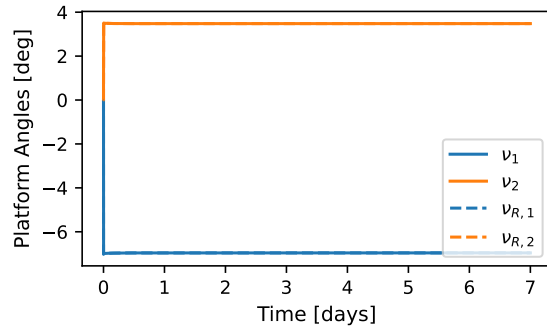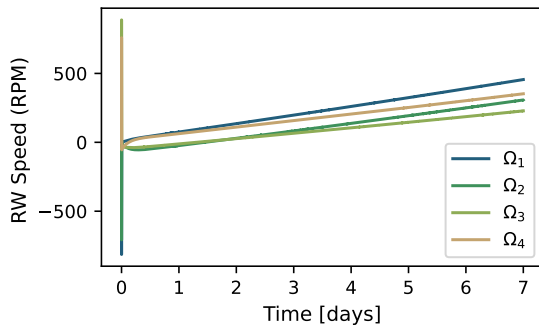
(b) Platform angles and reference vs time

(c) Wheels speeds vs time
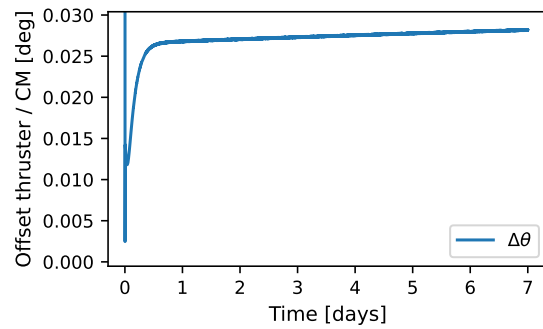
(d) Angular thruster - CM offset vs time
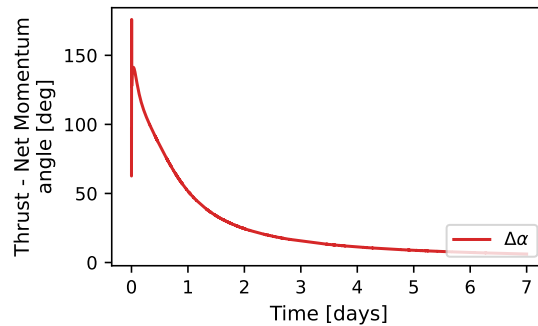
(e) Angular thruster - net momentum offset vs time

Figure 10: Long-term SRP effect, $\kappa = 10^{-4}$ Hz

15

agement loop. Lastly, subfigure (d) shows that the angular offset between thrust vector and center of mass, although small, grows over time, as momentum keeps building on the wheels.

Momentum management with excessively large gain

This last subsections aims at showing a shortcoming the momentum management strategy derived in the previous section. It can be tempting to pick a relatively large gain κ to obtain a large offset vector $\boldsymbol{d}$, and therefore provide a torque that dumps momentum quickly. Figure 11 shows the simulation results obtained with $\kappa = 10^{-3}$ Hz. It can be observed that all the plots are affected by a significant amount of jitter around some nominal behavior. This happens due to the nature of the control law in Equation (27), which effectively acts as a proportional controller. Figure 11 is showing the result of a controller that is oscillating continuously about the zero position, without ever settling. Because the attitude reference generation algorithm depends on the thruster direction, the persistent oscillation of the platform causes a continuous shift in the attitude reference, which destabilizes the attitude control loop. As a result, the attitude also never converges, causing the same jitter to appear in the reaction wheels in subfigure (3), where the wheel speeds keep oscillating as the spacecraft tries to chase a shifting reference attitude. This example is shown to highlight the strong coupling between all these components. Specifically, for the momentum management loop, it is advisable to always choose relatively low gains, to avoid destabilizing the other control loops. With even larger values of κ than the one shown in this section, the resulting torque can become so large

(a) Attitude and attitude reference vs time

(b) Platform angles and reference vs time

(c) Wheels speeds vs time

(d) Angular thruster - CM offset vs time
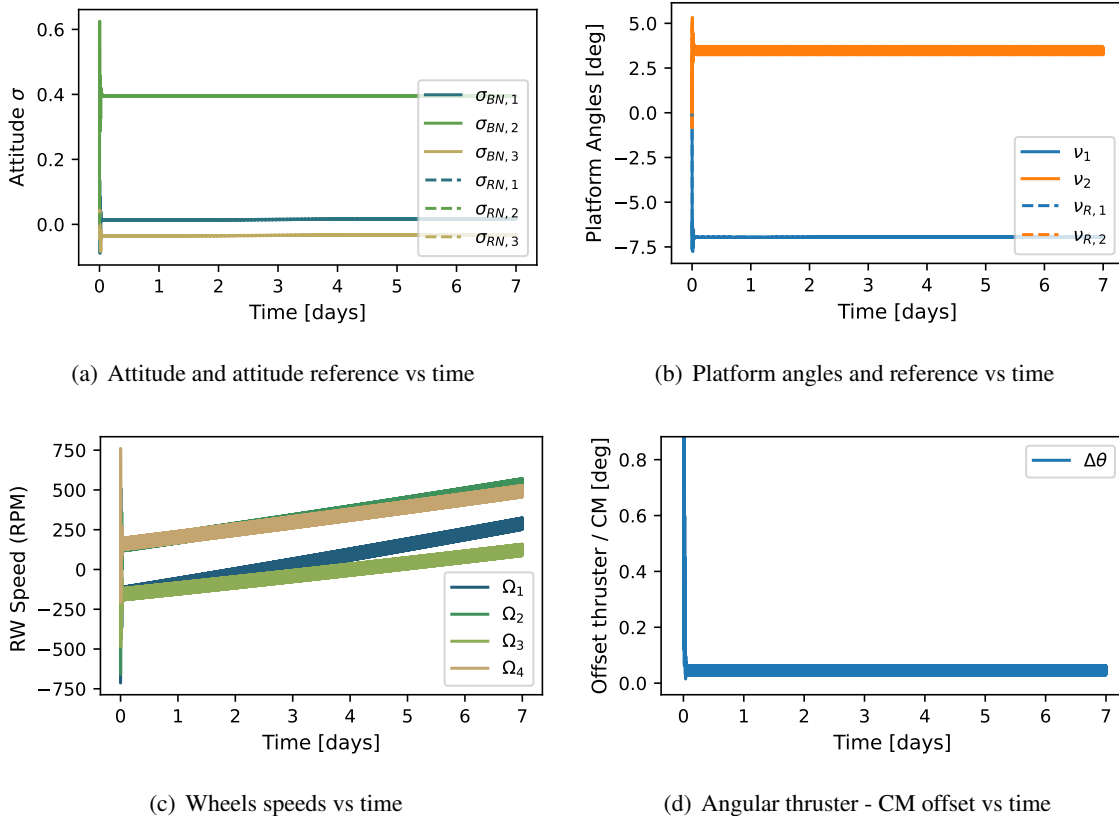
Figure 11: Long-term SRP effect, $\kappa = 10^{-3}$ Hz

that it can dump the momentum as the wheels are being actuated to perform attitude maneuvers, thus getting in the way of successfully controlling the spacecraft attitude. Alternatively, if a large gain is desired to dump momentum quickly, it is recommendable to run the momentum management loop at a lower frequency than other flight software segments, to prevent it from interfering with other high-frequency modes of the system.

CONCLUSIONS

This paper has shown the effects of solar radiation pressure on a spacecraft with large solar arrays, and how such phenomenon can cause the reaction wheels to saturate if no action is taken. An algorithm has been developed to rotate a double-hinged platform, combined with a SEP thruster, in order to fire the thrust direction through a desired point in the spacecraft hub. Minor assumptions were made on the relative position of the thruster and platform with respect to the hub, and therefore the results are very general. Moreover, a simple proportional-like control law has been developed to compute an offset with respect to the center of mass, along which the thruster should be fired in order to dump the net momentum accumulated on the reaction wheels. Simulations have shown how, over the same time windows, when the momentum dumping law is applied, the wheel speeds grow at a significantly slower rate. Moreover, simulations concur with such control law, in that they show the impossibility of dumping the net momentum in its entirety, because the component along the thrust direction cannot be controlled. Ultimately, the high fidelity of the simulation, featuring all the cross-couplings between dynamic components, has highlighted aspect of the control law that need to be kept in mind, regarding the frequency at which the control law should be updated and the gain that should be used in order to keep the system from destabilizing.

REFERENCES

[1] C. Früh, T. M. Kelecy, and M. K. Jah, "Coupled orbit-attitude dynamics of high area-to-mass ratio (HAMR) objects: influence of solar radiation pressure, Earth's shadow and the visibility in light curves," *Celestial Mechanics and Dynamical Astronomy*, Vol. 117, 2013, pp. 385–404.

[2] H. Schaub and J. L. Junkins, *Analytical Mechanics of Space Systems*. Reston, Virginia: American Institute of Aeronautics and Astronautics, Inc., 4 ed., 2018.

[3] A. K. Banerjee, N. Pedreiro, and W. E. Singhose, "Vibration reduction for flexible spacecraft following momentum dumping with/without slewing," *Journal of Guidance, Control, and Dynamics*, Vol. 24, No. 3, 2001, pp. 417–427.

[4] N. Pedreiro, "Spacecraft architecture for disturbance-free payload," *Journal of guidance, Control, and Dynamics*, Vol. 26, No. 5, 2003, pp. 794–804.

[5] M. A. Karami and F. Sassani, "Spacecraft momentum dumping using fewer than three external control torques," *Journal of guidance, control, and dynamics*, Vol. 32, No. 1, 2009, pp. 242–247.

[6] D. Tong, "Spacecraft momentum dumping using gravity gradient," *Journal of spacecraft and rockets*, Vol. 35, No. 5, 1998, pp. 714–717.

[7] E. A. Hogan and H. Schaub, "Three-axis attitude control using redundant reaction wheels with continuous momentum dumping," *Journal of Guidance, Control, and Dynamics*, Vol. 38, No. 10, 2015, pp. 1865–1871.

[8] D. Y. Oh, S. Collins, T. Drain, W. Hart, T. Imken, K. Larson, D. Marsh, D. Muthulingam, J. S. Snyder, D. Trofimov, *et al.*, "Development of the Psyche mission for NASA's Discovery Program," 2019.

[9] P. W. Kenneally, S. Piggott, and H. Schaub, "Basilisk: a flexible, scalable and modular astrodynamics simulation framework," *Journal of Aerospace Information Systems*, Vol. 17, No. 9, 2020, pp. 496–507.

[10] S. Carnahan, S. Piggott, and H. Schaub, "A New Messaging System For Basilisk," *AAS Guidance and Control Conference*, Breckenridge, CO, Jan. 30 – Feb. 5 2020. AAS 20-134.

[11] M. Cols-Margenet, H. Schaub, and S. Piggott, "Modular attitude guidance: Generating rotational reference motions for distinct mission profiles," *Journal of Aerospace Information Systems*, Vol. 15, No. 6, 2018, pp. 335–352.

[12] C. Rodriguez-Solano, U. Hugentobler, and P. Steigenberger, "Adjustable box-wing model for solar radiation pressure impacting GPS satellites," *Advances in Space Research*, Vol. 49, No. 7, 2012, pp. 1113–1128.